Space Weather

RESEARCH ARTICLE
10.1029/2024SW004297

Evidence of Substorm-Driven Penetration Electric Field Contributions to Low-Latitude Phenomena: Enhanced Upward Drifts, Plasma Bubble Development and Severe Scintillation

J. Sousasantos[1], F. S. Rodrigues[1], B. G. Fejer[2], R. W. Eastes[3], and A. O. Moraes[4,5]

[1]William B. Hanson Center for Space Sciences, The University of Texas at Dallas, Dallas, TX, USA, [2]Center for Atmospheric and Space Sciences, Utah State University, Logan, UT, USA, [3]Laboratory for Atmospheric and Space Physics, University of Colorado, Boulder, CO, USA, [4]Instituto de Aeronáutica e Espaço, São José dos Campos, Brazil, [5]Universidade de Taubaté, Taubaté, Brazil

Key Points:

- Impactful penetration electric fields from weaker substorms than previously proposed
- Penetration fields from such mild substorms increase vertical electron velocities and NmF2 in the early nighttime ionosphere
- Substorm onsets close to the evening can favor the development of plasma bubbles and severe scintillation on GNSS signals

Correspondence to:
J. Sousasantos,
jonas.ssts@utdallas.edu

Citation:
Sousasantos, J., Rodrigues, F. S., Fejer, B. G., Eastes, R. W., & Moraes, A. O. (2025). Evidence of substorm-driven penetration electric field contributions to low-latitude phenomena: Enhanced upward drifts, plasma bubble development and severe scintillation. *Space Weather*, *23*, e2024SW004297. https://doi.org/10.1029/2024SW004297

Received 3 DEC 2024
Accepted 14 FEB 2025

Author Contributions:
Conceptualization: J. Sousasantos, F. S. Rodrigues
Data curation: R. W. Eastes
Formal analysis: J. Sousasantos, F. S. Rodrigues, B. G. Fejer, R. W. Eastes, A. O. Moraes
Funding acquisition: J. Sousasantos
Investigation: J. Sousasantos
Methodology: J. Sousasantos
Project administration: J. Sousasantos
Supervision: J. Sousasantos
Visualization: J. Sousasantos
Writing – original draft: J. Sousasantos, F. S. Rodrigues, B. G. Fejer, R. W. Eastes, A. O. Moraes
Writing – review & editing: J. Sousasantos, F. S. Rodrigues, B. G. Fejer, R. W. Eastes, A. O. Moraes

Abstract In this work, it is demonstrated that substorm-driven penetration electric fields can efficiently enhance the upward plasma transport, favoring the development and structuring of plasma irregularities and the occurrence of scintillation on L-band signals. While most previous studies focus on investigating penetration electric fields during intense geomagnetic storms, here, the period used (April 01–05, 2020) was under very mild geomagnetic activity (-27 nT $\leq$ SYM-H ≤ 6 nT), so that interplanetary and disturbance dynamo contributions are minimized. This period comprised the same seasonal and solar flux conditions, while undergoing multiple short-lived substorms, making it well-suited to evaluate unequivocally: (a) to what extent substorm-driven penetration electric fields alter electrodynamical processes over low latitudes, and (b) how effective they are in contributing to the structuring of the early nighttime ionosphere and the subsequent occurrence of severe scintillation on L-band signals. Ground-based and space-based multi-instrument data sets were used. The results show that, even under weak geomagnetic activity, substorm-driven penetration electric fields—despite being subtle and short-lived—play a decisive role, enhancing the upward drifts, favoring the development of equatorial plasma bubbles and severe scintillation. The findings indicate that substorms with onsets coinciding with early nighttime are more impactful. This decisive contribution is more likely to be identified during late spring and early fall in the northern hemisphere (or vice versa in the southern hemisphere), when the prereversal vertical drifts are moderate—neither too small nor too large—and may have direct impacts on the day-to-day variability of equatorial plasma bubbles.

Plain Language Summary Most studies about the connection between events in the magnetosphere and ionosphere focus on periods with highly disturbed conditions and revealed that remarkable ionospheric phenomena are typically observed over low latitudes. During these events, however, the phenomena observed are likely to reflect contributions from multiple sources encompassed by the intricate solar-magnetospheric-ionospheric coupling. Consequently, a clear understanding about contributions from individual underlying mechanisms is difficult to achieve. In this work, we decided to explore this relatively under-researched topic. More specifically, we used ground-based and space-based data observed under very mild geomagnetic conditions—but with multiple short-lived substorms—to identify unambiguously the contributions from substorm-driven penetration electric fields to the formation of the structures known as Equatorial Plasma Bubbles (EPBs) and the occurrence of scintillation on L-band signals. We found that, despite being relatively subtle and short-lived, these penetration electric fields—that were overlooked in the past—can be decisive in regulating the occurrence of EPBs and scintillation, particularly when arising in the early nighttime. Our results also indicate that they may be a key factor in the day-to-day variability of EPBs, although their contribution would be more readily identified during specific seasonal and geomagnetic conditions.

1. Introduction

The role of the magnetosphere-ionosphere coupling in regulating the structuring of the low-latitude ionosphere during geomagnetic active periods has been subject of research for several decades. The first insights on this connection probably came from the studies of Matsushita (1954), Rastogi (1962), and Nishida (1968, 1971), followed by the works of Wolf and Jaggi (1973), Jaggi and Wolf (1973), and Onwumechili et al. (1973). The

unambiguous identification of the storm-time electric fields in data over low latitudes was first reported by Fejer et al. (1979) and Gonzales et al. (1979). Kelley et al. (1979) further expanded the discussion including considerations about northward turnings of the interplanetary magnetic field after a previously southward oriented state. The southward and subsequent northward oriented stages of the interplanetary magnetic field typically coincide to what today is usually referred to as "undershielding" and "overshielding" conditions, respectively, when the so-called "penetration electric fields" can reach low latitudes (Kikuchi et al., 1978, 1996).

Since the early days of the discovery that the magnetospheric-driven changes at high latitudes were connected to low latitudes, many studies were performed in an effort to understand and quantify the influence of these penetration electric fields in the low-latitude phenomenology (Huang et al., 2005, 2006, 2007; Kelley et al., 2003), and to demonstrate the consequences of the penetration electric fields over low latitudes through numerical simulation models (Huba et al., 2005). These studies indicated that only a fraction of the magnitude of the interplanetary penetrating electric fields reaches the equatorial region. That fraction is usually referred to as "efficiency factor" (e.g., Huang et al., 2007; Kelley et al., 2003; Kelley & Retterer, 2008). Therefore, the most drastic electrodynamical changes over low latitudes are expected to occur under strong geomagnetic activity. That is, perhaps, the reason why far more attention has been drawn to ionospheric phenomena during intense geomagnetic active periods. The periods of mild geomagnetic activity, on the other hand, have been considered as being devoid of significant contributions from the magnetosphere-ionosphere coupling. It is usually argued that the fraction of the penetration electric fields able to reach low latitudes under mild geomagnetic activity, in principle, would not cause noticeable changes in the ionospheric phenomena.

Recent works present evidence that, aside the influence of penetration electric fields during large geomagnetic storms, contributions from substorm-driven penetration electric fields are also important drivers of electrodynamical changes over low latitudes, especially near dusk and early nighttime (Fejer et al., 2021, 2024; Fejer & Navarro, 2022; Rout et al., 2019). Fejer et al. (2021), for instance, suggested that these substorm-driven penetration electric fields could enhance the prereversal drift velocities even during moderate geomagnetic activity. In a follow-up study, Fejer and Navarro (2022) used high time resolution upgraded Jicamarca radar drift observations to demonstrate that the equatorial electrodynamics is more sensitive to substorm-driven penetration electric fields than previously thought, and that substorms are, potentially, the main driving factors during extended intervals of steady southward oriented Bz. Fejer et al. (2024) analyzed the equatorial ionospheric responses to a geomagnetic storm in 23–24 April 2023 and found that the disturbance drift model proposed by Manoj and Maus (2012) underestimated the contribution from the penetration electric fields in most of the hours considered, suggesting that additional driving processes were needed to explain the electrodynamical changes observed over the equator. Fejer et al. (2024) also found evidence that substorm-driven short-lived penetration electric fields can be more prominent in the pre-midnight sector than in the daytime, that is, its impact in the early nighttime can be larger than what previous studies had proposed. Even with these recent research efforts, the longitudinal, latitudinal, and the solar flux dependence of these substorm-driven short-lived penetration electric fields are not completely understood.

In addition to that, because substorms very often coexist with changing interplanetary parameters, the unambiguous evaluation of their contribution to the equatorial electrodynamics is challenging. Under the intricate solar-magnetospheric-ionospheric coupling during moderate and strong geomagnetic activity, the prompt responses observed over low latitudes are likely to be a consequence of penetration electric fields driven by multiple sources. One possibility to isolate the contribution of substorm-driven penetration electric fields to the equatorial electrodynamics is to analyze data observed during periods of very mild geomagnetic activity.

In this work, ground-based and space-based multi-instrument data obtained during a period under very mild geomagnetic activity are used in an effort to unequivocally assess: (a) to what extent substorm-driven penetration electric fields change the electrodynamical processes over low latitudes; and (b) how effective substorm-driven penetration electric fields are in contributing to the structuring of the early nighttime low-latitude ionosphere and the subsequent occurrence of severe ionospheric scintillation on the Global Navigation Satellite System (GNSS) signals. The main processes and phenomena to be studied are the transport of the ionosphere to higher altitudes and the related vertical component of the plasma drift, the corresponding development of equatorial spread-F/Equatorial Plasma Bubbles (EPBs), and the ensuing ionospheric scintillation on GNSS signals. To do so, data from Digisonde, ground-based scintillation monitors and from the Global-scale Observations of the Limb and Disk (GOLD) instrument (Eastes et al., 2017) were used in association with solar wind parameters as obtained

from the Advanced Composition Explorer (ACE), and magnetic field indices from the SuperMAG database. The next sections present, respectively, details about the data sets, instruments and methods used, the results and discussion, and the concluding remarks.

2. Instruments, Data Sets and Methods

In order to evaluate the contribution of the substorm-driven penetration electric fields to the evolution of the low-latitude ionospheric plasma transport to higher altitudes and the resulting density irregularities and scintillation, data from 5 consecutive nights were analyzed. The nights used were April 01–05, 2020. These nights are well-suited to allow the proposed analysis of isolated contributions from substorm-driven penetration electric fields for the following reasons: (a) they are consecutive nights, therefore not suffering from seasonal or solar flux changes; (b) the period selected was either geomagnetically quiet or under very mild geomagnetic activity; and (c) the nights belong to the end of the spread-F season over the longitudes considered, and EPBs were not expected to be observed due to the low solar flux conditions (F10.7 $\approx$ 70 solar flux units, and the GOLD daily average Q_{EUV} was between 1.281 and 1.306, in erg cm^{-2} s^{-1}). An inspection of GOLD images (not shown here) revealed that the last noticeable EPB occurrence over the region considered was on 20 March 2020.

The data used was obtained from the Digisonde deployed in Fortaleza, Brazil (geographic longitude: 38.54°W, geographic latitude: 3.72°S, dip latitude: 8.76°S). The data was manually scaled using the SAO Explorer software, and the information used were the true height of the peak of the F-region density (hmF2) and the vertical drift derived therefrom as (dhmF2/dt). It must be mentioned that the location of the Digisonde is slightly off-equator, therefore, it is reasonable to assume that the estimated altitude of the peak of the F-region density (hmF2) and the upward vertical drift are smaller than the actual values over the dip equator (e.g., Abdu et al., 2009; Sousasantos et al., 2020). Consequently, the values are more qualitative in that regard.

The GOLD data used was the F-region peak density (Level 2—NMAX), typically referred to as NmF2. The GOLD observations cover the early nighttime over the longitudes considered and are well-suited to evaluate at least two aspects of the ionosphere related to this work. The first is the location of the Equatorial Ionization Anomaly (EIA), which is a qualitative measure of the vertical transport of plasma over the dip equator through the Fountain Effect. The second is the unambiguous detection of the occurrence of large-scale plasma density irregularities. The observations used correspond to hours around 23:10 UT (~20:30 LT). The frames were selected based on the time at which spread-F was first observed in the ionograms from the Digisonde.

Ground-based scintillation measurements from a monitor Septentrio PolaRx5S located in Natal, Brazil (geographic longitude: 35.20°W, geographic latitude: 5.84°S, dip latitude: 12.60°S) were also used. The monitor is part of the INCT/CIGALA/CALIBRA network (de Paula et al., 2023; Monico et al., 2022). The information used was the amplitude scintillation index S_4 (Ryle & Hewish, 1950; Yeh & Liu, 1982), that can be defined as the standard deviation of $I/\langle I \rangle$, where I is the received signal intensity, and the brackets represent ensemble averages. The standard deviation and average were estimated using signal measurements sampled at 50 Hz over intervals of 60 s. Only data observed by satellites with elevation angles $\geq$20° were used. The station and the elevation angle criterion were chosen so that the field of view (FOV) encompasses the location of the Digisonde station while also having several Ionospheric Pierce Points (IPPs) on the locations where EPBs were observed by the GOLD instrument. At the same time, the elevation angle constraint avoids the use of data suffering from multipath errors.

The interplanetary parameters used were the GSM interplanetary magnetic (Bz) and electric (Ey) field components obtained at the High-Resolution OMNI (HRO) (King & Papitashvili, 2005, 2010, 2013), available at https://omniweb.gsfc.nasa.gov/form/omni_min.html. The geomagnetic indices used were the SYM-H, equivalent to the Dst index but with higher resolution (e.g., Wanliss & Showalter, 2006), and the SuperMAG SML and SMU indices (equivalent to the AL and AU indices) obtained at http://supermag.jhuapl.edu/ (Newell & Gjerloev, 2011). The SML and SMU indices were derived from 1-min resolution data observed by approximately 300 ground-based magnetometers (Gjerloev, 2012).

3. Results and Discussion

The results and the discussion are presented in next four subsections. First, an analysis about the early nighttime background ionospheric conditions for the nights considered is presented, discussing the distinct trends observed on April 02 and 03, 2020. In the sequence, the structuring of the ionosphere and the development of EPBs under

the enhanced upward drifts on April 02 and 03, 2020, is discussed. The third subsection presents the results and discussion related to the evolution of the ionospheric scintillation on the nights considered, showing that only on April 02 and 03 ionospheric scintillation occurred. Finally, the fourth subsection shows evidence supporting the hypothesis that the enhanced upward drifts observed on April 02 and 03, 2020, and the subsequent development of EPBs and severe ionospheric scintillation were primarily due to substorm-driven penetration electric fields.

3.1. Dissimilar Evolution of the F-Region Altitudes in the Early Nighttime

Figure 1 shows 5 "profilograms", that is, graphical representations of the vertical electron density profiles over time as observed by the Digisonde. Each panel from (a)–(e) corresponds to the profilogram over the early nighttime for the nights of April 01–05, 2020, respectively. The electron density values are detailed by the colors at the right-hand side color bar. The black dashed line corresponds to the electron density peak height (hmF2). The values up to hmF2 were observed, but the values above the peak are modeled by the SAO Explorer software. The gray bars on panels (b) and (c) represent the hours when spread-F was observed in the ionograms. Only early nighttime hours between 20:00 UT–23:50 UT (∼17:26 LT–21:16 LT over the station) were considered, so that the periods with the most drastic changes in the equatorial ionosphere is covered, including the Prereversal enhancement (PRE) of the vertical drift (e.g., Farley et al., 1986) and the typical generation of EPBs and scintillation (Sousasantos, Moraes, et al., 2024).

On the nights of April 01, 04, and 05, 2020 (panels a, d, and e, respectively) a very subtle elevation of the ionosphere up to about 21:20 UT (∼18:46 LT) can be noticed, but only in the lowest portion of the profiles. As the hmF2 altitudes highlight, that was not efficient on transporting the ionosphere upward, and the general trend is of downward motion with time. Therefore, the PRE was very weak and, as expected, no spread-F occurred in any of these nights.

On the nights of April 02 and 03, 2020 (panels b and c, respectively), on the other hand, the upward motion was clearly enhanced when compared to the other nights, especially around the PRE peak time, and the development of spread-F was observed on the subsequent ionograms. These variations in the altitudes of the F-region over the nights considered have a close relation to the changes in the eastward electric field over the dip equator. Since the profiles belong to consecutive nights under the same seasonal and solar flux conditions, it is likely that these short-lived changes were driven by external contributions such as penetration electric fields.

Figure 2 shows a more rigorous analysis focusing on the temporal evolution of the hmF2 and the associated vertical drift (dhmF2/dt) during the early nighttime over the 5 nights considered. Panel (a) exhibits the hmF2 for the 5 nights with black lines representing the nights with no spread-F occurrence and red and magenta lines indicating the hmF2 for April 02, 2020, and April 03, 2020, respectively, as described by the legend. The vertical blue dashed line demarcates the hour when the upward trend on the red and magenta lines started to be noticed (20:30 UT, i.e., ∼17:56 LT).

The results on panel (a) show, with no ambiguity, that while on April 01 (black solid line), 04 (black dashed line), and 05 (black dotted line) the F-region was transported mostly downward, on April 02 (red solid line) and 03 (magenta line) the F-region was clearly transported upward. The difference in altitudes reached more than 74 km (contrasting April 03 and 05 at 21:50 UT, i.e., ∼19:16 LT). On panel (b) the same hmF2 information was used to derive the vertical drift velocities (v = dhmF2/dt). The vertical drift values for April 01, 04, and 05 are mostly negative (downward), but on April 02 and 03 the values are positive, and a clear PRE can be noticed, reaching values close to ∼15 m/s. As mentioned earlier, the Digisonde station is slightly off-equator (dip latitude 8.76°S), therefore, the actual hmF2 and PRE values over the dip equator can be expected to be larger than those presented in Figure 2.

The important result to be emphasized here is that on April 02 and 03, 2020, the considerably different plasma vertical transport was presumably driven by penetration electric fields. Later it will be demonstrated that these were substorm-driven penetration electric fields under very mild geomagnetic activity. In the next subsections the results will show that these subtle substorm-driven contributions led to drastic changes in terms of EPB development and ionospheric scintillation.

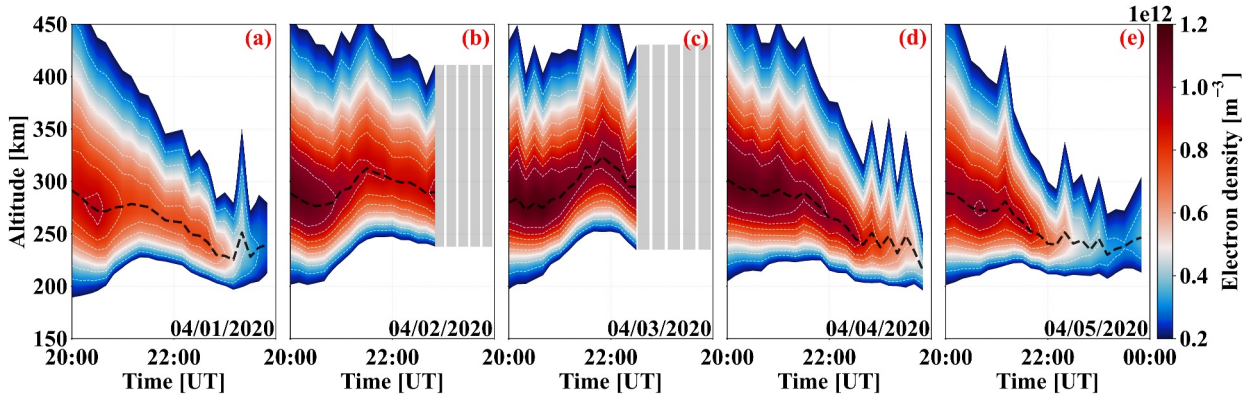

Figure 1. Profilograms obtained from the Digisonde deployed at Fortaleza. The panels (a)–(e) show the profiles of the electron density (colors) with altitude in the early nighttime and the hmF2 (black dashed line) for the nights between 04/01–04/05, respectively. The gray bars denote the periods under spread-F. It must be mentioned that the values up to the profile peak density (hmF2) were observed, but the values above the peak are modeled by the SAO Explorer software.

3.2. The Development of EPBs Under the Enhanced F-Region Upward Drift

As demonstrated in the previous section, on April 02 and 03, 2020, the PRE was considerably larger when compared to all the other nights considered. Previous works proposed that spread-F and EPBs only evolve when the PRE vertical drift peak reaches a given threshold. In an early work, Abdu et al. (1983) suggested a value of 15 m/s as this threshold. Later, Abdu et al. (2009), using data from the Conjugate Point Equatorial Experiment (COPEX), proposed a threshold of 22 m/s. The results from Kil et al. (2009) also indicate that, for a probability of EPB occurrence ≥50%, the minimum threshold value required is ∼20 m/s. According to the discussion presented earlier it is legitimate to assume that on April 02 and 03 that threshold was reached over the dip equator. If the reasoning above is correct, EPBs must be absent on April 01, 04, and 05, but must be observed on April 02 and 03. Recent studies have suggested that seeding source disturbances, resulting from forcing from below, could counterbalance a weak or absent PRE (e.g., Yizengaw & Groves, 2020), thereby providing favorable conditions for EPB development. However, in the cases presented here, it is important to reiterate that on April 02 and 03, in contrast to the other nights, the F-region was elevated to higher altitudes, and the threshold for the PRE vertical drift peak was reached (prior to spread-F occurrence), therefore not requiring any additional counterbalancing forcing from below.

To confirm unambiguously the absence/occurrence of EPBs on the nights considered, data from GOLD is presented on the panels of Figure 3. Panels (a)–(e) show the NmF2 observations for the nights of April 01–05, respectively. The hour of the observations used on these panels is 23:10 UT (∼20:30 LT) and corresponds approximately to the time when spread-F was first observed in the Digisonde data. The NmF2 values are

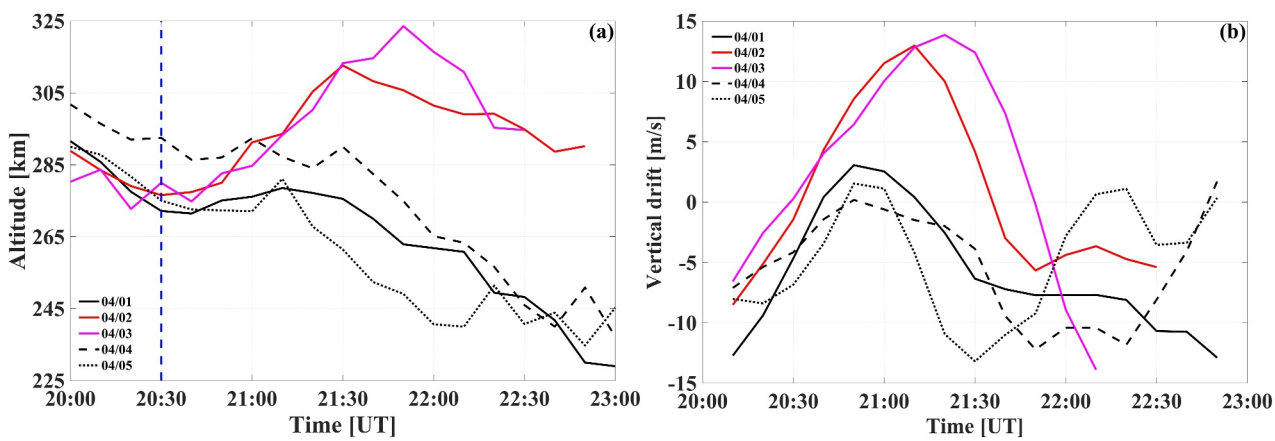

Figure 2. Profiles of hmF2 (a) and the corresponding vertical drift (b) for the nights considered. A clear difference can be noticed for 04/02 and 04/03, when substorm onsets coincided with the local evening and early nighttime as will be presented later in this work.

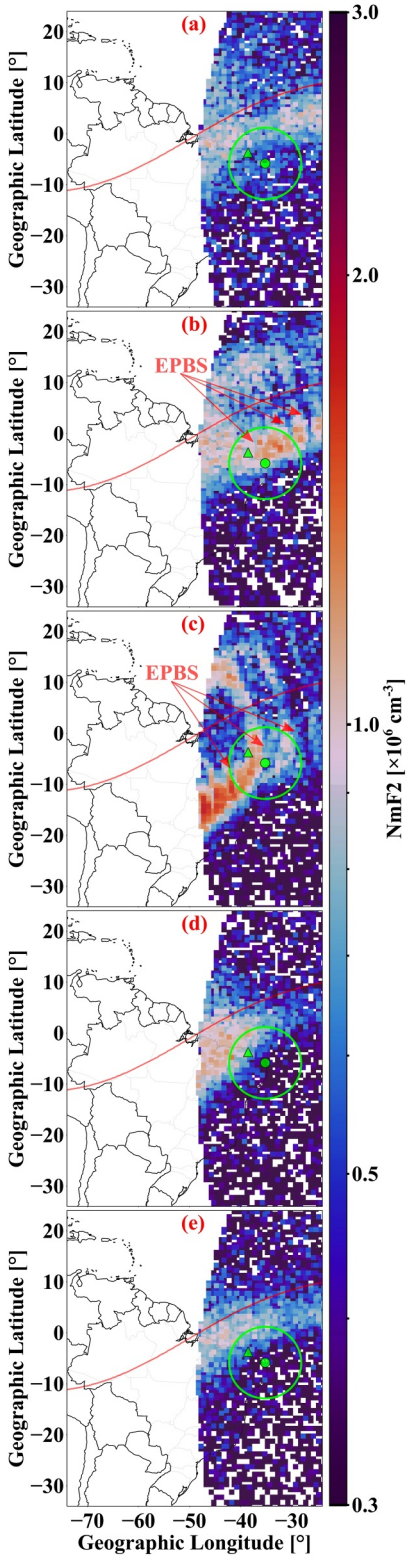

Figure 3. GOLD NmF2 data (colors) confirming the presence of EPBs on 04/02 and 04/03 (panels b and c) and the absence of EPBs on all the other nights (panels a, d, and e). The green dot and the green circle depict the location of the scintillation monitor station (Natal) and the field of view considered. The green triangle represents the Digisonde station of Fortaleza. The red solid line shows the dip equator.

described by the color bar at the right-hand side. The red solid line indicates the dip equator. The green dot shows the location of the scintillation monitor and the green circle describes the field of view considering elevation angles ≥20°. The green triangle corresponds to the location of the Digisonde station.

On panels (a), (d), and (e) two results can be readily noticed. The first is that the Equatorial Ionization Anomaly (EIA) crests are considerably more contracted equatorward when compared to the panels (b) and (c). That is a direct confirmation of the results presented in the previous subsection and substantiate the hypothesis that additional driving processes increased the eastward electric fields in the early nighttime on April 02 and 03, 2020, which resulted in an enhanced Fountain Effect. The second important result is that on April 02 (panel b) and 03 (panel c) EPBs were observed, while no EPBs occurred on all the other nights. Also, it is worth notice that on April 03, 2020 (panel c) the EIA crests had the most poleward latitudes and the EPBs are more well-developed. Therefore, the differences in the upward drifts and F-region altitudes during the early nighttime, as discussed in the previous subsection, favored the development of EPBs, as confirmed by the GOLD data. A consequence of these results is that subtle additional drivers can lead to considerable differences in terms of EPB development. The primary additional driver will be demonstrated to be substorm-driven penetration electric fields in a later subsection.

3.3. The Occurrence of Severe Scintillation on April 02 and 03, 2020

In the previous subsections, the results demonstrated that on April 02 and 03, 2020, the early nighttime upward plasma transport was significantly greater when compared to the other nights considered. It was also shown that the enhanced upward drifts on April 02 and 03 favored the development of EPBs. In addition, these enhanced upward drifts possibly contributed to sustaining the ionospheric background density over the early nighttime hours. In the hours when EPBs were observed, the peak electron densities estimated from the GOLD data (1.12×10^6, 1.45×10^6, 1.80×10^6, 1.35×10^6, and 1.06×10^6 cm^{-3}, for April 01–05, respectively) were up to ∼37% and ∼70% higher on April 02 and 03, respectively, compared to April 05.

It is known that the ionospheric background density plays a crucial role in determining the severity of the ionospheric scintillation (Sousasantos, Rodrigues, et al., 2024). To evaluate to what extent the variations observed have led to changes in the scintillation levels, the S_4 values on the nights considered are presented in Figure 4. Both L-band frequencies, L1 (∼1.6 GHz) and L2 (∼1.2–1.3 GHz) are shown in black and red, respectively. The horizontal black dashed line highlights the threshold $S_4 = 0.2$, above which the signals are considered as being affected by ionospheric scintillation. Only data observed with elevation angles ≥20° were used.

At the one hand, on the nights of April 01, 04 and 05, 2020, not a single case of $S_4 > 0.2$ occurred. On the other hand, on April 02, 2020, the occurrence of S_4 reaching ∼0.7 indicates the development of moderate-to-severe scintillation. On April 03, 2020, the S_4 incidence was even more pronounced, reaching values of about 1.2, which is considered extremely severe (Sreeja et al., 2020). Therefore, the differences in velocity and altitude observed on April 02 and 03 (see Figure 2), although not extreme, drastically changed the scintillation environment for the GNSS signals.

In order to demonstrate unambiguously that the scintillation observed was caused by the plasma density deviations related to the EPBs, Figure 5 shows

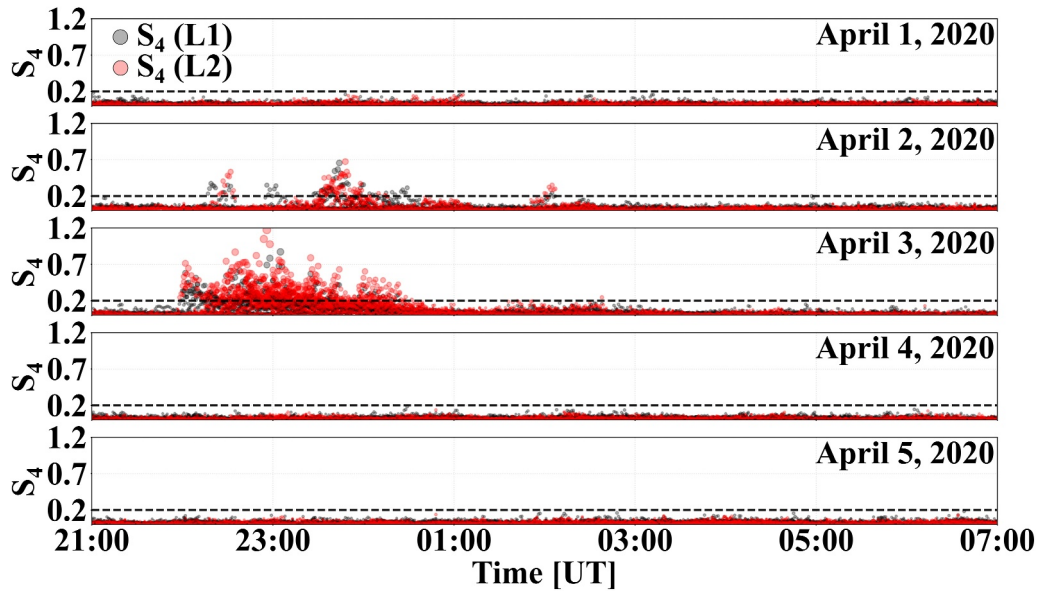

Figure 4. Scintillation index for the nights between 04/01–04/05 (upper to lower panels, respectively). The black/red dots indicate the S_4 on L1/L2 signals.

the "skymap" of the S_4 (L2) at the IPPs observed by the scintillation monitor in Natal. Only the nights of April 02 and 03, 2020, are shown on the left and right panels, respectively. The colors (and sizes) of the dots are related to the S_4 values described by the color bar at the right-hand side.

On both nights the larger S_4 values are mostly concentrated at the north and northeast portions of the field of view, especially at the northeast. These are the same regions of the sky where EPBs were observed by GOLD, as shown in Figure 3, therefore, it is legitimate to state that the scintillation observed was caused by the EPBs generated under more favorable conditions on April 02 and 03, 2020.

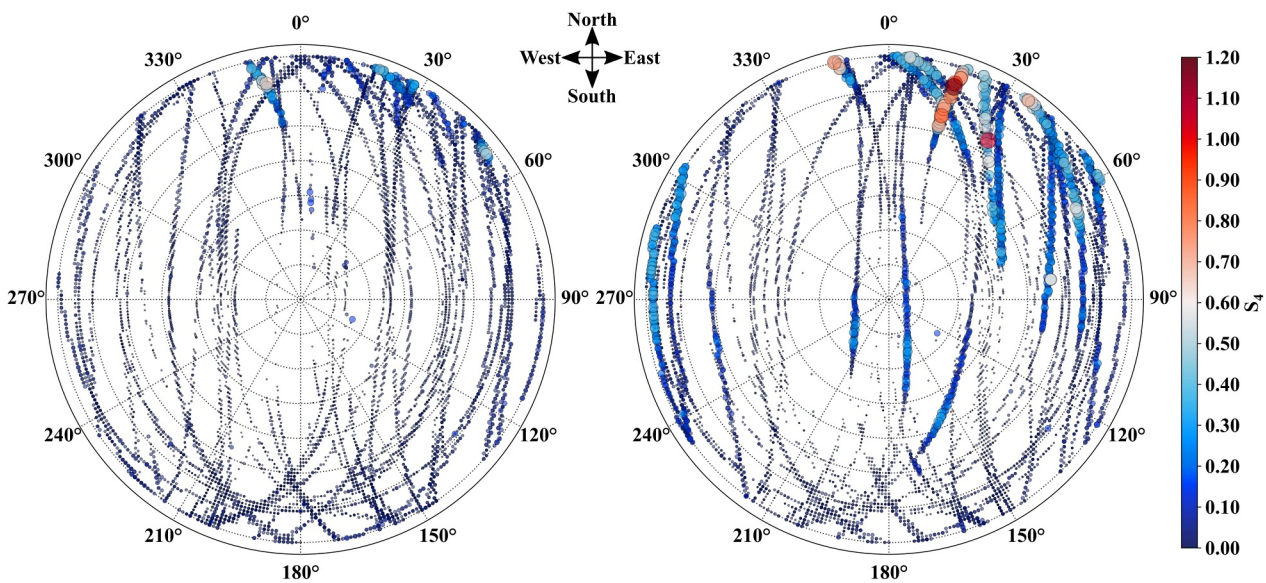

Figure 5. Skymaps of the IPPs observed in Natal for 04/02 (left) and 04/03 (right) showing the occurrence of moderate-to-severe and extremely severe scintillation, respectively. The locations of the scintillation events are in conformity with those of EPBs on GOLD data (Figure 3).

3.4. Evidence for Substorm-Driven Penetration Electric Fields as the Driving Process

The results presented in the previous subsections depict a clear interrelationship involving: (a) enhanced upward drifts on April 02 and 03, 2020, indicating some additional driving process, unlike the other nights considered; (b) the development of EPBs under these enhanced upward drifts; and (c) the occurrence of moderate-to-severe and extremely severe scintillation on April 02 and 03, 2020, respectively, while all the other nights had no scintillation for either of the GNSS L-band frequencies. Because the analyses considered subsequent nights under the same seasonal and solar flux conditions, and since the changes observed seem to be short-lived, the most likely driving process providing additional upward forcing could be penetration electric fields. However, as mentioned earlier, the period selected was under very mild geomagnetic activity, therefore, substorm-driven penetration electric fields must be considered. Substorm-driven penetration electric fields mechanisms are not fully understood to date (e.g., Hui et al., 2017; Maruyama, 2020), with the penetration effect being assumed as caused by an imbalance between Region I and Region II field-aligned currents (Maruyama, 2020). The exact manner in which substorms generate this imbalance, however, remains unclear.

To investigate in more detail the geomagnetic conditions during the observations reported here, the interplanetary Bz and Ey components are shown in the upper panel of Figure 6, the SYM-H index in the middle panel, and the SuperMAG auroral current indices SMU and SML (Newell & Gjerloev, 2011) in the lower panel. The upper horizontal axis is local time (LT) at Fortaleza.

The upper panel shows that the values of Bz (red line) and Ey (black line) were, in general, very small, with $-5.99\ \text{nT} \leq \text{Bz} \leq 5.92\ \text{nT}$, and $-2.48\ \text{mV/m} \leq \text{Ey} \leq 2.62\ \text{mV/m}$, respectively. In the middle panel, the SYM-H index corroborates that the period was under very mild geomagnetic conditions, with $-27\ \text{nT} \leq \text{SYM-H} \leq 6\ \text{nT}$. During the period analyzed the largest value for Kp (not shown here) was 3.7 during 21:00-23:00 UT on April 03, 2020, which is classified as only "unsettled" (e.g., Filjar, 2008). According to Loewe and Prölss (1997), a weak geomagnetic storm requires, in general, at least levels of Kp ≥4 and SYM-H/Dst ≤−36 nT. All these interplanetary parameters and geomagnetic indices confirm that the period analyzed was under very mild geomagnetic activity. Additionally, if the "efficiency factor" values proposed in previous works (e.g., Huang et al., 2007; Kelley et al., 2003; Kelley & Retterer, 2008) are considered, it is unlikely that contributions from Ey would lead to effective penetration electric fields.

The lower panel shows the SMU and SML indices. The blue shaded regions indicate the evening/early nighttime on each night (between 17:00 LT and 21:00 LT at Fortaleza), referencing to the approximate hours when the upward drift enhancement was noticed in the results of panel (a) of Figure 2, i.e., the time when the contributing driving process was unambiguously perceived. In the lower panel of Figure 6, colors were used as a visual resource to highlight the transition in the values of SMU and SML indices. These indices show that, although the period was under very mild geomagnetic activity, the auroral indices had several short-lived steep increases, all under southward Bz conditions. The red arrows indicate substorm onsets during the evening and early nighttime on April 02 and 03, 2020, identified by the Newell and Gjerloev substorm criteria (Gjerloev, 2012; Newell & Gjerloev, 2011). The black arrows indicate all the other substorm onsets also identified by the Newell and Gjerloev substorm criteria. Newell and Gjerloev (2011) considered SML (and AL) 1-min cadence data using a 30-mintes sliding buffer and identify an onset at a given time (t_0) if 4 conditions are satisfied: (a) $\text{SML}(t_0 + 1) - \text{SML}(t_0) < -15$ nT; (b) $\text{SML}(t_0 + 2) - \text{SML}(t_0) < -30$ nT; (c) $\text{SML}(t_0 + 3) - \text{SML}(t_0) < -45$ nT; and (d) $\sum_{i=4}^{i=30} \text{SML}(t_0 + i)/26 - \text{SML}(t_0) < -100$ nT. More specifically, the onset is identified whenever a sharp and sustained drop is observed, and it is assumed to take place at the last minute before condition (a) happens. All the methods used to identify substorms are limited in some way, as informed at the SuperMAG website and mentioned by Fejer and Navarro (2022). More recently, however, Lao et al. (2024) showed evidence that the Newell and Gjerloev technique is one of the best available to identify substorm onsets.

One important aspect of the information presented in the lower panel is that the substorm onsets (with considerable auroral current indices) only coincided with evening and early nighttime hours on April 02 and 03, 2020. More specifically, on April 02, 2020, the substorm onsets occurred at ∼19:31 UT and 23:10 UT (∼16:57 LT and 20:52 LT). On April 03, 2020, the substorm onsets were at ∼20:19 UT, 21:59 UT, and 22:40 UT (∼17:45 LT, 19:25 LT, and 20:06 LT). These substorm onsets started approximately when the PRE is expected to occur near Fortaleza (e.g., Abdu et al., 2009; Fejer et al., 1991).

10.1029/2024SW004297

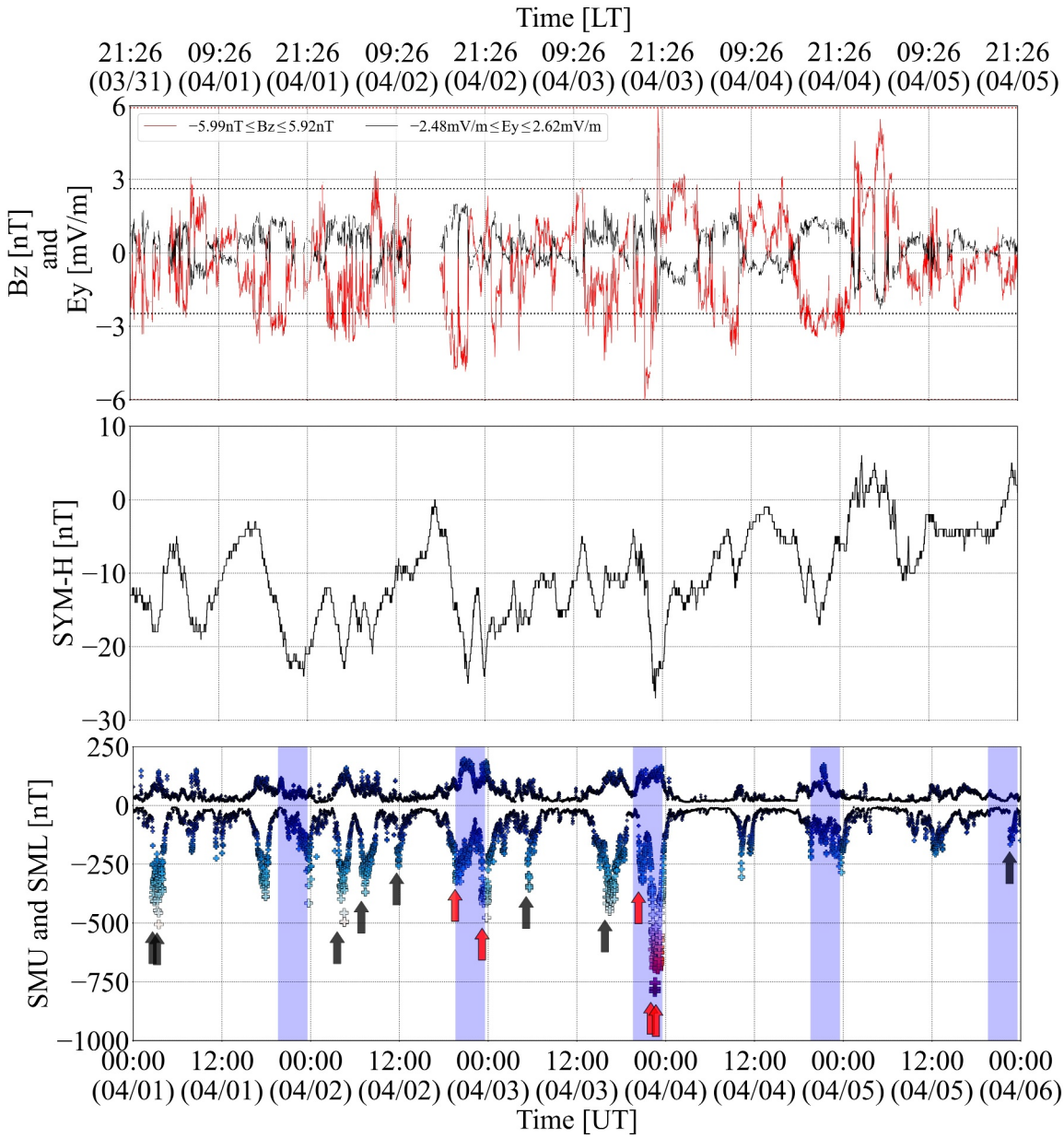

Figure 6. Interplanetary and geomagnetic conditions during the nights considered in this study. Upper panel: Interplanetary Bz (red line) and Ey (black line) components. Middle panel: SYM-H index. Lower panel: SuperMAG SMU and SML indices. The blue shaded regions indicate the evening/early nighttime period. The red arrows highlight the onset of substorms on early nighttime of April 02 and 03, 2020, according to the Newell and Gjerloev technique. The black arrows show the other occurrences of substorm onsets.

These results confirm the findings of Fejer and Navarro (2022) and illustrate the impact of substorm-driven penetration electric fields during the evening and early nighttime hours. The results show that these electric fields are very efficient in modulating the vertical plasma transport, even if they are relatively weak and short-lived. Most importantly, since the geomagnetic activity was very mild throughout the period considered, the results correspond to an unambiguous evaluation of the isolated contribution of substorm-driven penetration electric fields to the equatorial electrodynamics. Therefore, as mentioned in previous subsections, the substorm-driven penetration electric fields were the most likely driving process contributing to the enhanced upward drifts, favoring the development of plasma bubbles and severe scintillation. A potential consequence of these results is that these underlying contributions, which have been overlooked, can be one of the key factors in regulating the day-to-day variability of EPBs, a subject critical to contemporary geospace and space weather studies. These

substorm contributions are likely to be more easily identified during late spring and early fall in the northern hemisphere (or vice versa in the southern hemisphere), when the prereversal vertical drifts are moderate—neither too small nor too large. This will be investigated in more depth in future work.

4. Conclusion

In this work ground-based and space-based multi-instrument data obtained during April 01–05, 2020, were analyzed to assess: (a) to what extent substorm-driven penetration electric fields change the electrodynamical processes at low latitudes; and (b) how effective substorm-driven penetration electric fields are in contributing to the structuring of the early nighttime low-latitude ionosphere and the subsequent occurrence of severe ionospheric scintillation on the GNSS signals. In order to identify the substorm-driven contribution unequivocally, the period selected for the analyses was under very mild geomagnetic conditions (-5.99 nT $\leq$ Bz $\leq$ 5.92 nT, -2.48 mV/m $\leq$ Ey $\leq$ 2.62 mV/m, and -27 nT $\leq$ SYM-H $\leq$ 6 nT). At the same time, multiple short-lived substorms took place throughout the period selected, making it exceptionally well-suited for the evaluations proposed.

Among all the substorm events considered, only two had onsets coinciding with the evening and early nighttime over the longitudes considered. That happened on the nights of April 02 and 03, 2020. The striking result is that only on those two nights, unlike the previous and subsequent nights, the electrodynamics over low latitudes was considerably altered, with enhanced upward drifts during the PRE hours, what favored the development of EPBs and, ultimately, led to moderate-to-severe and extremely severe scintillation on GNSS signals on April 02 and 03, 2020, respectively.

The main conclusions can be summarized as follows.

1. After evaluating a period under very mild geomagnetic activity, the results indicate, unequivocally, that even with no significant disturbed time electric fields from interplanetary and disturbance dynamo origin, several short-lived substorm-driven penetration electric fields drove upward drifts and increased NmF2 altitudes over low latitudes.
2. Despite being subtle and short-lived, these substorm-driven penetration electric fields altered considerably the electrodynamical processes over low latitudes, especially when their onsets are during the evening and early nighttime. The contribution from these substorm-driven penetration electric fields can be sufficient to change drastically the phenomenology at low latitudes. The additional contribution to the upward drifts in the evening and early nighttime seems to be critical in defining the subsequent structuring of the equatorial and low-latitude ionosphere.
3. Penetration electric fields during very mild substorms were previously considered to have negligible impact. However, the results presented here demonstrate that they play a crucial role, favoring the development of EPBs and the occurrence of severe scintillation on GNSS signals in a period that, otherwise, would be devoid of such phenomena.

Data Availability Statement

The Digisonde data is publicly available at: https://giro.uml.edu/didbase/. The Global-Observations of the Limb and Disk data is publicly available at: https://gold.cs.ucf.edu/data/ and at the NASA's Space Physics Data Facility (SPDF) https://spdf.gsfc.nasa.gov/pub/data/gold/. The scintillation data is publicly available at: https://ismr-querytool.fct.unesp.br/is/#. The interplanetary parameters are publicly available at: https://omniweb.gsfc.nasa.gov/form/omni_min.html. The SMU and SML indices and substorm lists are publicly available at: https://supermag.jhuapl.edu/.

Acknowledgments

J. Sousasantos acknowledges NASA award 80NSSC24K0563. F. S. Rodrigues acknowledges NSF Award AGS-2122639 and NASA award 80NSSC24K0563. R. W. Eastes acknowledges NASA Contract 80GSFC18C0061 to the University of Colorado, Boulder. A. O. Moraes acknowledges CNPq award PQ 309389/2021-6. Monitoring stations from the INCT GNSS NavAer network were deployed in the context of the INCT GNSS NavAer, CNPq project number 465648/2014-2, CAPES project number 23038.000776/2017-54 and FAPESP Project Number 2017/50115-0. We acknowledge the substorm timing list identified by the Newell and Gjerloev technique (Newell & Gjerloev, 2011), the SMU and SML indices (Newell & Gjerloev, 2011); and the SuperMAG collaboration (Gjerloev, 2012). Also, we gratefully acknowledge the SuperMAG collaborators (https://supermag.jhuapl.edu/info/?page=acknowledgement). We acknowledge use of NASA/GSFC's Space Physics Data Facility's OMNIWeb (or CDAWeb or ftp) service, and OMNI data (King & Papitashvili, 2005, 2010, 2013).

References

Abdu, M. A., Batista, I. S., Reinisch, B. W., de Souza, J. R., Sobral, J. H. A., Pedersen, T. R., et al. (2009). Conjugate Point Equatorial Experiment (COPEX) campaign in Brazil: Electrodynamics highlights on spread F development conditions and day-to-day variability. *Journal of Geophysical Research*, *114*(A4), 1–21. https://doi.org/10.1029/2008JA013749

Abdu, M. A., de Medeiros, R. T., Bittencourt, J. A., & Batista, I. S. (1983). Vertical ionization drift velocities and range type spread F in the evening equatorial ionosphere. *Journal of Geophysical Research*, *88*(A1), 399–402. https://doi.org/10.1029/JA088iA01p00399

de Paula, E. R., Monico, J. F. G., Tsuchiya, I. H., Valladares, C. E., Costa, S. M. A., Marini-Pereira, L., et al. (2023). A retrospective of global navigation satellite system ionospheric irregularities monitoring networks in Brazil. *Journal of Aerospace Technology and Management*, *15*(e0123), 1–17. https://doi.org/10.1590/jatm.v15.1288

Eastes, R. W., McClintock, W. E., Burns, A. G., Anderson, D. N., Andersson, L., Codrescu, M., et al. (2017). The global-scale observations of the limb and disk (GOLD) mission. *Space Science Reviews*, *212*(1–2), 383–408. https://doi.org/10.1007/s11214-017-0392-2

Farley, D. T., Bonelli, E., Fejer, B. G., & Larsen, M. F. (1986). The prereversal enhancement of the zonal electric field in the equatorial ionosphere. *Journal of Geophysical Research*, *91*(A12), 13723–13728. https://doi.org/10.1029/JA091iA12p13723

Fejer, B. G., de Paula, E. R., González, S. A., & Woodman, R. F. (1991). Average vertical and zonal drifts over Jicamarca. *Journal of Geophysical Research*, *96*(A8), 13901–13906. https://doi.org/10.1029/91ja01171

Fejer, B. G., Gonzales, C. A., Farley, D. T., Kelley, M. C., & Woodman, R. F. (1979). Equatorial electric fields during magnetically disturbed conditions 1. The effect of the interplanetary magnetic field. *Journal of Geophysical Research*, *84*(A10), 5797–5802. https://doi.org/10.1029/JA084iA10p05797

Fejer, B. G., Laranja, S. R., & Condor, P. (2024). Multi-process driven unusually large equatorial perturbation electric fields during the April 2023 geomagnetic storm. *Frontiers in Astronomy and Space Sciences*, *11*, 1–9. https://doi.org/10.3389/fspas.2024.1351735

Fejer, B. G., & Navarro, L. A. (2022). First observations of equatorial ionospheric electric fields driven by storm-time rapidly recurrent magnetospheric substorms. *Journal of Geophysical Research: Space Physics*, *127*(12), 1–8. https://doi.org/10.1029/2022JA030940

Fejer, B. G., Navarro, L. A., Sazykin, S., Newheart, A., Milla, M. A., & Condor, P. (2021). Prompt penetration and substorm effects over Jicamarca during the September 2017 geomagnetic storm. *Journal of Geophysical Research: Space Physics*, *126*(8), 1–11. https://doi.org/10.1029/2021JA029651

Filjar, R. (2008). A study of direct severe space weather effects on GPS ionospheric delay. *Journal of Navigation*, *61*(1), 115–128. https://doi.org/10.1017/S0373463307004420

Gjerloev, J. W. (2012). The SuperMAG data processing technique. *Journal of Geophysical Research*, *117*(A9), 1–19. https://doi.org/10.1029/2012JA017683

Gonzales, C. A., Kelley, M. C., Fejer, B. G., Vickrey, J. F., & Woodman, R. F. (1979). Equatorial electric fields during magnetically disturbed conditions 2. Implications of simultaneous auroral and equatorial measurements. *Journal of Geophysical Research*, *84*(A10), 5803–5812. https://doi.org/10.1029/ja084ia10p05803

Huang, C., Sazykin, I., Spiro, R., Goldstein, J., Crowley, G., & Ruohoniemi, J. M. (2006). Storm-time penetration electric fields and their effects. *Eos, Transactions American Geophysical Union*, *87*(13), 131. https://doi.org/10.1029/2006EO130005

Huang, C. S., Foster, J. C., & Kelley, M. C. (2005). Long-duration penetration of the interplanetary electric field to the low-latitude ionosphere during the main phase of magnetic storms. *Journal of Geophysical Research*, *110*(A11), 1–13. https://doi.org/10.1029/2005JA011202

Huang, C. S., Sazykin, S., Chau, J. L., Maruyama, N., & Kelley, M. C. (2007). Penetration electric fields: Efficiency and characteristic time scale. *Journal of Atmospheric and Solar-Terrestrial Physics*, *69*(10–11), 1135–1146. https://doi.org/10.1016/j.jastp.2006.08.016

Huba, J. D., Joyce, G., Sazykin, S., Wolf, R., & Spiro, R. (2005). Simulation study of penetration electric field effects on the low-to mid-latitude ionosphere. *Geophysical Research Letters*, *32*(23), 1–4. https://doi.org/10.1029/2005GL024162

Hui, D., Chakrabarty, D., Sekar, R., Reeves, G. D., Yoshikawa, A., & Shiokawa, K. (2017). Contribution of storm time substorms to the prompt electric field disturbances in the equatorial ionosphere. *Journal of Geophysical Research: Space Physics*, *122*(5), 5568–5578. https://doi.org/10.1002/2016JA023754

Jaggi, R. K., & Wolf, R. A. (1973). Self-consistent calculation of the motion of a sheet of ions in the magnetosphere. *Journal of Geophysical Research*, *78*(16), 2852–2866. https://doi.org/10.1029/JA078i016p02852

Kelley, M. C., Fejer, B. G., & Gonzales, C. A. (1979). An explanation for anomalous equatorial ionospheric electric fields associated with a northward turning of the interplanetary magnetic field. *Geophysical Research Letters*, *6*(4), 301–304. https://doi.org/10.1029/gl006i004p00301

Kelley, M. C., Makela, J. J., Chau, J. L., & Nicolls, M. J. (2003). Penetration of the solar wind electric field into the magnetosphere/ionosphere system. *Geophysical Research Letters*, *30*(4), 1–3. https://doi.org/10.1029/2002GL016321

Kelley, M. C. ; J., & Retterer, J. (2008). First successful prediction of a convective equatorial ionospheric storm using solar wind parameters. *Space Weather*, *6*(8), 1–4. https://doi.org/10.1029/2007SW000381

Kikuchi, T., Araki, T., Maeda, H., & Maekawa, K. (1978). Transmission of polar electric fields to the equator. *Nature*, *273*(5664), 650–651. https://doi.org/10.1038/273650a0

Kikuchi, T., Lühr, H., Kitamura, T., Saka, O., & Schlegel, K. (1996). Direct penetration of the polar electric field to the equator during a DP 2 event as detected by the auroral and equatorial magnetometer chains and the EISCAT radar. *Journal of Geophysical Research*, *101*(A8), 17161–17173. https://doi.org/10.1029/96ja01299

Kil, H., Paxton, L. J., & Oh, S. J. (2009). Global bubble distribution seen from ROCSAT-1 and its association with the evening prereversal enhancement. *Journal of Geophysical Research*, *114*(A6), 1–9. https://doi.org/10.1029/2008JA013672

King, J., & Papitashvili, N. (2010). One min and 5-min solar wind data sets at the Earth's bow shock nose. Retrieved from http://omniweb.gsfc.nasa.gov/html/HROdocum.html

King, J. H., & Papitashvili, N. (2005). Solar wind spatial scales in and comparisons of hourly Wind and ACE plasma and magnetic field data. *Journal of Geophysical Research*, *110*, A02104. https://doi.org/10.1029/2004JA010649

King, J. H., & Papitashvili, N. E. (2013). OMNI combined, definitive, 1-minute IMF and plasma data time-shifted to the nose of the earth's bow shock, plus magnetic indices. *AdnetSystems, NASA GSFC*. Retrieved from https://cdaweb.gsfc.nasa.gov/

Lao, C. J., Forsyth, C., Freeman, M. P., Smith, A. W., & Mooney, M. K. (2024). On the association of substorm identification methods. *Journal of Geophysical Research: Space Physics*, *129*(9), 1–16. https://doi.org/10.1029/2024JA032762

Loewe, C. A., & Prölss, G. W. (1997). Classification and mean behavior of magnetic storms. *Journal of Geophysical Research*, *102*(A7), 14209–14213. https://doi.org/10.1029/96JA04020

Manoj, C., & Maus, S. (2012). A real-time forecast service for the ionospheric equatorial zonal electric field. *Space Weather*, *10*(9), 1–9. https://doi.org/10.1029/2012SW000825

Maruyama, N. (2020). Chapter 9 – Storms and substorms—The new whole system approach and future challenges. In *The dynamical ionosphere* (pp. 87–119). Elsevier. https://doi.org/10.1016/B978-0-12-814782-5.00009-1

Matsushita, S. (1954). Ionospheric variations associated with geomagnetic disturbances I. Variations at moderate latitudes and the equatorial zone, and the current system for the S_D field. *Journal of Geomagnetism and Geoelectricity*, *5*(4), 109–135. https://doi.org/10.5636/jgg.5.109

Monico, J. F. G., de Paula, E. R., Moraes, A. O., Costa, E., Shimabukuro, M. H., Alves, D. B. M., et al. (2022). The GNSS NavAer INCT project overview and main results. *Journal of Aerospace Technology and Management*, *14*(e0722), 1–23. https://doi.org/10.1590/jatm.v14.1249

Newell, P. T., & Gjerloev, J. W. (2011). Evaluation of SuperMAG auroral electrojet indices as indicators of substorms and auroral power. *Journal of Geophysical Research*, *116*(A12), 1–15. https://doi.org/10.1029/2011JA016936

Nishida, A. (1968). Coherence of geomagnetic DP 2 fluctuations with interplanetary magnetic variations. *Journal of Geophysical Research*, *73*(17), 5549–5559. https://doi.org/10.1029/JA073i017p05549

Nishida, A. (1971). DP 2 and polar substorm. *Planetary and Space Science*, *19*(2), 205–221. https://doi.org/10.1016/0032-0633(71)90200-5

Onwumechili, A., Kawasaki, K., & Akasofu, S. I. (1973). Relationships between the equatorial electrojet and polar magnetic variations. *Planetary and Space Science*, *21*(1), 1–16. https://doi.org/10.1016/0032-0633(73)90015-9

Rastogi, R. G. (1962). The effect of geomagnetic activity on the F_2 region over central Africa. *Journal of Geophysical Research*, *67*(4), 1367–1374. https://doi.org/10.1029/JZ067i004p01367

Rout, D., Pandey, K., Chakrabarty, D., Sekar, R. ; X., & Lu, X. (2019). Significant electric field perturbations in low latitude ionosphere due to the passage of two consecutive ICMEs during 6–8 September 2017. *Journal of Geophysical Research: Space Physics*, *124*(11), 9494–9510. https://doi.org/10.1029/2019JA027133

Ryle, M., & Hewish, A. (1950). The effects of the terrestrial ionosphere on the radio waves from discrete sources in the galaxy. *Monthly Notices of the Royal Astronomical Society*, *110*(4), 381–394. https://doi.org/10.1093/mnras/110.4.381

Sousasantos, J., Abdu, M. A., Santos, A., Batista, I., Silva, A., & Loures, L. E. (2020). Further complexities on the pre-reversal vertical drift modeling over the Brazilian region: A comparison between long-term observations and model results. *Journal of Space Weather and Space Climate*, *10*(20), 1–9. https://doi.org/10.1051/swsc/2020022

Sousasantos, J., Moraes, A. O., Di Santis, V., & Vani, B. C. (2024). Temporal characterization of pre-midnight fading events over low latitudes. *Advances in Space Research*, *73*(1), 794–806. https://doi.org/10.1016/j.asr.2023.10.034

Sousasantos, J., Rodrigues, F. S., Moraes, A. O., Eastes, R. W., & Monico, J. F. G. (2024). On the estimation of scintillation severity using background F-region peak densities: Description and example results using GOLD observations. *GPS Solutions*, *28*(62), 1–11. https://doi.org/10.1007/s10291-023-01602-6

Sreeja, V. V., Aquino, M., Marques, H. A., & Moraes, A. O. (2020). Mitigation of ionospheric scintillation effects on GNSS precise point positioning (PPP) at low latitudes. *Journal of Geodesy*, *94*(15), 1–10. https://doi.org/10.1007/s00190-020-01345-z

Wanliss, J. A., & Showalter, K. M. (2006). High-resolution global storm index: Dst versus SYM-H. *Journal of Geophysical Research*, *111*(A2), 1–10. https://doi.org/10.1029/2005JA011034

Wolf, R. A., & Jaggi, R. K. (1973). Can the magnetospheric electric field penetrate to the low-latitude ionosphere? Comments on astrophysics and. *Space Physics*, *5*, 99.

Yeh, K. C., & Liu, C. H. (1982). Radio wave scintillations in the ionosphere. *Proceedings of the IEEE*, *70*(4), 324–360. https://doi.org/10.1109/PROC.1982.12313

Yizengaw, E., & Groves, K. (2020). Forcing from lower thermosphere and quiet time scintillation longitudinal dependence. *Space Weather*, *18*(11), 1–13. https://doi.org/10.1029/2020SW002610